The Astrophysical Journal Letters, 871:L3 (7pp), 2019 January 20 https://doi.org/10.3847/2041-8213/aaf9b6

Unusual Isotopic Abundances in a Fully Convective Stellar Binary

I. J. M. Crossfield[1], J. D. Lothringer[2], B. Flores[1,3], E. A. C. Mills[4], R. Freedman[5,6], J. Valverde[1,7,8], B. Miles[9], X. Guo[1], and A. Skemer[9]
[1] Department of Physics, and Kavli Institute for Astrophysics and Space Research, Massachusetts Institute of Technology, Cambridge, MA, USA; iancross@mit.edu
[2] Lunar and Planetary Laboratory, University of Arizona, Tucson, AZ, USA
[3] Department of Physics and Astronomy, California State University Northridge, Northridge, CA, USA
[4] Department of Physics, Brandeis University, Waltham, MA, USA
[5] NASA Ames Research Center, Moffett Field, CA, USA
[6] SETI Institute, Mountain View, CA, USA
[7] Department of Physics, University of California, Santa Cruz, Santa Cruz, CA, USA
[8] Chabot-Las Positas Community College, Dublin, CA, USA
[9] Department of Astronomy, University of California, Santa Cruz, Santa Cruz, CA, USA
Received 2018 November 9; revised 2018 December 17; accepted 2018 December 18; published 2019 January 17

Abstract

Low-mass M dwarfs represent the most common outcome of star formation, but their complex emergent spectra hinder detailed studies of their composition and initial formation. The measurement of isotopic ratios is a key tool that has been used to unlock the formation of our solar system, the Sun, and the nuclear processes within more massive stars. We observed GJ 745AB, two M dwarfs orbiting in a wide binary, with the NASA Infrared Telescope Facility/iSHELL spectrograph. Our spectroscopy of CO in these stars at the 4.7 μm fundamental and 2.3 μm first-overtone rovibrational bandheads reveals $^{12}C^{16}O$, $^{13}C^{16}O$, and $^{12}C^{18}O$ in their photospheres. Because the stars are fully convective, the atomic constituents of these isotopologues should be uniformly mixed throughout the stars' interiors. We find that in these M dwarfs, both $^{12}C/^{13}C$ and $^{16}O/^{18}O$ greatly exceed the Solar values. These measurements cannot be explained solely by models of Galactic chemical evolution, but require that the stars formed from an interstellar medium significantly enriched by material ejected from an exploding core-collapse supernova. These isotopic measurements complement the elemental abundances provided by large-scale spectroscopic surveys, and open a new window onto studies of Galactic evolution, stellar populations, and individual systems.

Key words: infrared: stars – techniques: spectroscopic – stars: abundances – supernovae: general

Supporting material: data behind figure

1. Introduction and Observations

Detailed analysis of the thermal emission spectra of stars smaller, cooler, and lower-mass than the Sun is significantly more challenging than for hotter, brighter stars. These M dwarfs are relatively faint, emit most of their energy at wavelengths beyond the visible, and their atmospheres are cool enough to contain numerous molecules with many spectral features. Nonetheless, these cool objects are subjects of considerable study, both because they represent the single most common outcome of star formation and because they appear to be especially likely to host planetary systems (Dressing & Charbonneau 2015). By characterizing the chemical properties of M dwarfs, we learn about the chemical enrichment and star formation history of our own Milky Way galaxy, and hope to also learn about the formation of planetary systems, including some of the best targets for studying potentially habitable planets.

We used the iSHELL spectrograph (Rayner et al. 2016) on the NASA Infrared Telescope Facility (IRTF) to observe GJ 745A and B, two otherwise indistinguishable M dwarfs with radii, masses, and metallicity all roughly a third that of the Sun (see Table 1). Both stars should be chemically homogeneous throughout, because they are fully convective. The stars lie just 0.05 mag in brightness, and 0.05 dex in luminosity, below a newly identified gap in the lower main sequence that separates fully convective M dwarfs from those that are only partially convective (Jao et al. 2018; MacDonald & Gizis 2018).

We observed GJ 745A and B on the night of UT 2017 July 2 (Program 2017A110, PI: I. J. M. Crossfield), acquiring $R = 70{,}000$ (4.3 km s^{-1}) spectroscopy and mostly continuous coverage from 4.52 to 5.24 μm. The full details of our observations are listed in Table 1. Conditions were photometric throughout the night.[10] We reduced the raw iSHELL data using the `SpeXTool` Data Reduction package (Cushing et al. 2004). `SpeXTool` flat-fields raw images to correct for pixel-to-pixel variations and uses sky emission lines in science frames for the wavelength calibration. The calibrated *M*-band frames were then nod-subtracted (to remove sky emission and hot pixels) and stacked to produce a set of master frames for each star. After calibrating this master frame, spatial profiles are computed, two 1D spectra are extracted (one at each nod position), and the two spectra are combined to produce a single spectrum for each star.

We then correct for telluric absorption features by using the observed A0V standard star (HR 7390), the science target star (GJ 745A or B), and a high-resolution model spectrum of Vega

[10] As shown by the Canada France Hawaii Telescope Skyprobe atmospheric transparency data archive, http://www.cfht.hawaii.edu/cgi-bin/elixir/skyprobe.pl?plot&mcal_20170702.png.

Table 1
System and Observational Parameters

Parameter	GJ 745A	GJ 745B	References
SpT	M2V	M2V	
M_{K_s} [mag]	6.657 ± 0.021	6.652 ± 0.023	Skrutskie et al. (2006), Gaia Collaboration et al. (2018)
M_{W2} [mag]	6.399 ± 0.022	6.417 ± 0.031	Cutri et al. (2012), Gaia Collaboration et al. (2018)
ϖ [mas]	113.34 ± 0.10	113.21 ± 0.05	Gaia Collaboration et al. (2018)
d [pc]	8.821 ± 0.008	8.831 ± 0.004	Bailer-Jones et al. (2018)
$T_{\rm eff}$ [K]	3454 ± 31	3440 ± 31	Houdebine (2010), Gaidos & Mann (2014), Mann et al. (2015), Newton et al. (2015)
R_* [$R_\odot$]	0.32 ± 0.01	0.33 ± 0.01	Houdebine (2010), Gaidos & Mann (2014), Mann et al. (2015), Newton et al. (2015)
M_* [$M_\odot$]	0.31 ± 0.03	0.31 ± 0.03	Gaidos & Mann (2014), Mann et al. (2015), Benedict et al. (2016)
$\log_{10}[L_*/L_\odot]$	−1.88 ± 0.03	−1.91 ± 0.03	This work
$v \sin i$ [km s^{-1}]	<3	<3	Jenkins et al. (2009), Houdebine (2010)
[Fe/H] [dex]	−0.43 ± 0.05	−0.39 ± 0.05	Mann et al. (2015), Newton et al. (2015)
^{12}C/H [10^{-4}]	1.04 ± 0.03	0.995 ± 0.05	This work
^{13}C/H [10^{-7}]	3.5 ± 0.5	4.5 ± 0.4	This work
^{18}O/H [10^{-7}]	1.7 ± 0.4	1.3 ± 0.3	This work
^{12}C/^{13}C	296 ± 45	224 ± 26	This work
^{16}O/^{18}O	1220 ± 260	1550 ± 360	This work
iSHELL Mode	M1	M1	
Slit	0.″375 × 15″	0.″375 × 15″	
Guiding filter	K	K	
Integration time [s]	14.83	14.83	
Non-destructive reads	1	1	
Co-adds	3	3	
Exposures	100	102	
UT times	08:19–09:47	10:35–12:06	
Slit position angle	−84.°9–88.°6	−108.°1 to +99.°5	
Airmass range	1.22–1.03	1.00–1.05	
A0V airmass range	1.05–1.01		

(Vacca et al. 2004). Since A0V stars have spectra that are nearly featureless, the A0V spectrum corrects the object spectra. We also tune the depths and widths of hydrogen absorption lines in the model to better match HR 7390 and minimize residuals at these wavelengths. Although HR 7390 rotates more rapidly than Vega and is somewhat cooler, both of these factors are accounted for in the `SpeXTool` reduction: the former by convolving the Vega model spectrum with a rotational broadening kernel, and the latter by adjusting the spectral slope based on the star's $(B-V)$ color. Finally, we remove parts of the spectrum with obvious bad pixels and wherever signal-to-noise ratio (S/N) < unity. In practice, the choice of S/N cut-off is not especially significant as low-S/N parts of the spectrum are appropriately de-weighted when we calculate our weighted-mean line profile for each isotopologue.

2. Modeling

2.1. Stellar Spectra

To measure the ^{12}C/^{13}C isotopic ratio of GJ 745A and B we compare our observed spectra to synthetic spectra generated from custom atmosphere models of the two stars, both spectra and models being derived from the PHOENIX atmosphere code (Version 16, Husser et al. 2013). Our PHOENIX model atmospheres contain 64 vertical layers, spaced evenly in log-space on an optical depth grid from $\tau = 10^{-10}$ to 100, spanning 1.0–10^5 nm. In our observed wavelength range, the models were sampled at least every 0.01 nm. The models were run with H I, He I–II, C I–IV, N I–IV, O I–IV, Mg I–III, and Fe I–IV in NLTE. We ran models using the stellar parameters listed in Table 1 for five different ^{12}C/^{13}C ratios—29.3, 89.9, 271.7, 908.1, and 2731.2, corresponding to ^{13}C enrichments of 3×, 1×, 1/3×, 1/10×, and 1/30× solar, respectively—and three different ^{16}O/^{18}O ratios—165.3, 498.8, and 1497.7, corresponding to ^{18}O enrichments of 3×, 1×, and 1/3× solar, respectively. We use a CO line list (Goorvitch 1994) that contains lines for ^{12}C^{16}O, ^{13}C 16, ^{12}C^{17}O, ^{12}C^{18}O, ^{13}C^{18}O, ^{14}C^{16}O, and ^{13}C^{17}O.

We verify our isotopic measurement by comparing a PHOENIX model of the Sun to high-resolution spectra from Kitt Peak's Fourier-Transform Spectrograph (Hase et al. 2010). Our Solar model gives an excellent match to the known solar isotopic ratios. Including the atoms listed above in non-local thermodynamic equilibrium (NLTE) in the Solar model changes the line depths of CO isotopologues by 0.3%, negligible compared to our current measurement uncertainty.

2.2. Measuring Isotopic Ratios

The highest-S/N regions of our spectra are 4.6–4.7 μm, where tellurics are relatively weak and stellar spectra are dominated by ^{12}C^{16}O lines. We used the HITEMP database (Rothman et al. 2010) to identify ^{13}CO and C^{18}O lines that are relatively clear of tellurics and other strong absorption lines, as listed in Table 2. Most of the ^{13}CO lines are individually visible but all have fairly low statistical significance, while the individual C^{18}O lines can only barely be discerned by eye. To boost our S/N we construct a single line profile by taking the weighted mean of each line (after linearly continuum-normalizing each line using the regions listed in Table 2). The resulting mean line profiles, shown in Figure 1, clearly reveal the strong signature of both ^{13}CO and the rarer C^{18}O in both GJ 745A and B.

Table 2
CO Lines Used in This Work

λ_0 (Å)	Species	Transition Details				Continuum Regions[a]			
		ν'	ν''	Branch	J	L_L	L_R	R_L	R_R
23374.128	$^{12}C^{16}O$	2	0	R	4	−3.1	−2.1	1.6	2.5
23393.233	$^{12}C^{16}O$	2	0	R	3	−1.9	−1.3	1.7	2.2
23412.752	$^{12}C^{16}O$	2	0	R	2	−4.5	−2.5	1.3	1.7
23432.695	$^{12}C^{16}O$	2	0	R	1	−1.5	−0.6	0.6	1.9
23727.167	$^{12}C^{16}O$	3	1	R	1	−5.0	−4.0	1.8	2.5
46116.476	$^{13}C^{16}O$	1	0	R	21	−9.0	−2.0	5.0	7.0
46178.775	$^{13}C^{16}O$	1	0	R	20	−8.0	−5.5	2.0	5.5
46205.730	$^{13}C^{16}O$	2	1	R	29	−0.9	−0.65	1.0	2.5
46241.999	$^{13}C^{16}O$	1	0	R	19	−5.0	−2.5	4.0	6.0
46317.954	$^{13}C^{16}O$	2	1	R	27	−4.5	−1.5	4.2	6.5
46404.576	$^{13}C^{16}O$	3	2	R	36	−4.0	−1.5	1.0	2.0
46433.864	$^{13}C^{16}O$	2	1	R	25	−5.0	−1.5	5.0	9.0
46556.783	$^{13}C^{16}O$	3	2	R	33	−8.0	−4.5	1.5	3.8
46641.064	$^{13}C^{16}O$	1	0	R	13	−3.0	−1.3	1.4	2.5
46710.901	$^{13}C^{16}O$	1	0	R	21	−4.0	−3.0	2.0	4.0
46717.315	$^{13}C^{16}O$	3	2	R	30	−3.5	−1.2	2.0	5.0
46926.227	$^{13}C^{16}O$	1	0	R	9	−4.0	−1.5	1.5	3.0
46935.010	$^{13}C^{16}O$	2	1	R	17	−3.5	−1.8	2.0	5.5
46030.116	$^{12}C^{18}O$	2	1	R	34	−3.5	−1.0	1.0	2.5
46133.337	$^{12}C^{18}O$	2	1	R	32	−4.5	−1.3	3.6	4.6
46144.648	$^{12}C^{18}O$	1	0	R	22	−1.8	−0.8	0.8	1.4
46186.304	$^{12}C^{18}O$	2	1	R	31	−4.5	−1.5	1.0	2.5
46240.182	$^{12}C^{18}O$	2	1	R	30	−2.1	−1.1	0.5	4.0
46594.024	$^{12}C^{18}O$	1	0	R	15	−2.6	−1.0	0.8	1.7
46704.254	$^{12}C^{18}O$	2	1	R	22	−4.0	−1.0	1.0	2.5
46871.567	$^{12}C^{18}O$	1	0	R	11	−1.9	−0.9	1.0	4.0
46893.682	$^{12}C^{18}O$	2	1	R	19	−4.0	−1.0	1.0	2.5
47016.125	$^{12}C^{18}O$	1	0	R	9	−2.1	−1.0	1.0	2.1
47024.717	$^{12}C^{18}O$	2	1	R	17	−4.0	−0.5	0.5	4.0

Note.
[a] Left (L) and right (R) edges of the left- and right-hand regions used for linear continuum normalization; all values are relative to λ_0, in Å.

We measure the $^{13}C/H$ and $^{18}O/H$ abundance ratios for each star by interpolating our grid of PHOENIX models so as to minimize the χ^2 calculated from the mean observed and modeled lines (after removing a linear pseudocontinuum as described above). We infer 1σ confidence intervals using the region where $\Delta\chi^2 \leqslant$ unity (Avni 1976). We find that the accessible ^{12}CO lines in the fundamental band are too strongly saturated to tightly constrain the stars' $^{12}C/H$ abundances, so we instead use weaker lines in the first overtone band from 2.1 to 2.5 μm iSHELL spectra of the binary taken on the same night.

To verify that using different CO lines in different bands does not bias our results, we compare the individual intensities of the lines used in our analysis from each of three sources: Goorvitch et al. (1994; still used in constructing our PHOENIX model spectra); HITEMP (Rothman et al. 2010); and a custom list constructed by Gordon et al. (R. Freedman 2018, private communication). We find clear evidence of systematic offsets in the (gf) values, with consistent offsets for each combination of isotopologue and line list. These numbers imply that the inferred isotopic abundances may suffer from systematic biases at the 2% level. As we currently measure $^{12}C/^{13}C$ to only 10% precision, this 2% effect does not significantly impact our current analysis.

With this approach, we measure [C/H] = −0.37 and −0.39 dex for GJ 745A and B, respectively—entirely consistent with their iron depletion of [Fe/H] = −0.4 dex. As CO is a poor measure of oxygen abundance, we use the [C/H] and [O/H] abundances observed in M dwarfs (Tsuji 2016; Souto et al. 2017, 2018) to infer $^{16}O/H$. These observations include stars with a range of metallicities and are consistent with [O/H] = [C/H], so we assume this ratio also holds for our targets.

We find that the best-fit abundance ratios vary by roughly 5% depending on the particular lines that we use for stacking and the range of velocities that we use to calculate χ^2. We therefore assume an additional $(5\% \times \sqrt{2}) = 7.1\%$ systematic uncertainty for our isotopic measurements. Nonetheless, our total uncertainties are dominated by measurement noise.

2.3. Discussion

Our spectra clearly reveal multiple rare isotopologues of carbon monoxide (CO). ^{13}CO has been inferred from medium-resolution 2.3 μm spectroscopy, but $C^{18}O$ has not been measured in any dwarf stars beyond the Sun. For both $C^{18}O$ and ^{13}CO, we find isotopic abundance ratios significantly discrepant from the Solar values. Whereas the Sun has $^{12}C/^{13}C = 93.5 \pm 3.1$ and $^{16}O/^{18}O = 525 \pm 21$ (Lyons et al. 2018), for GJ745 A and B we find $^{12}C/^{13}C = 296 \pm 45$ and 224 ± 26, and $^{16}O/^{18}O = 1220 \pm 260$ and 1550 ± 360, respectively (see Table 1). The ratio of our $^{12}CO/^{13}CO$ and $C^{16}O/C^{18}O$ abundance ratios gives $^{13}CO/C^{18}O$, a quantity that is more accurately measured in

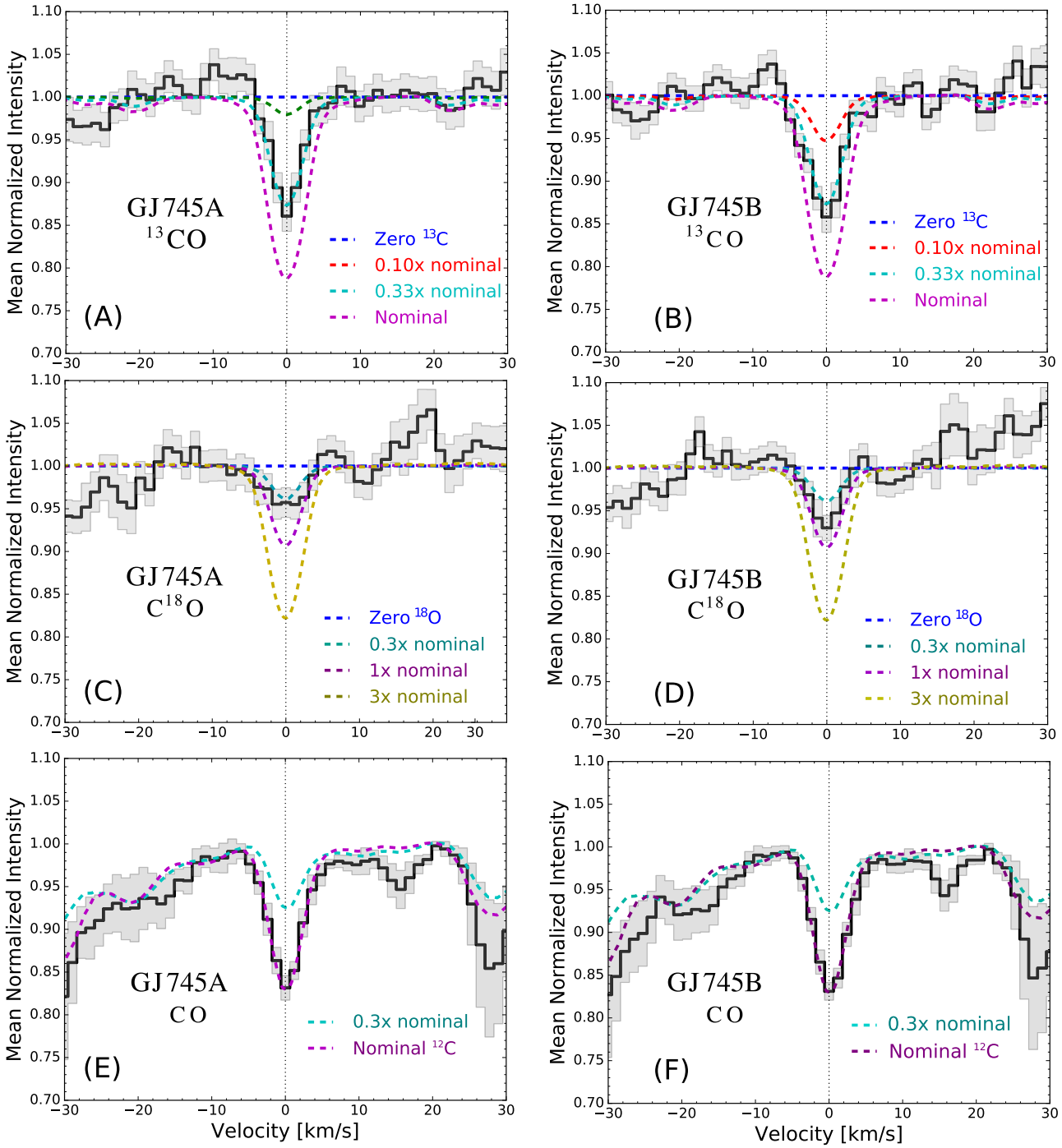

Figure 1. Stacked absorption lines of CO isotopologues in GJ 745AB, showing clear evidence of both ^{13}CO (panels (A) and (B)), C^{18}O (panels (C) and (D)), and the abundant ^{12}C^{16}O (panels (E) and (F)). The black curve and gray shaded region indicate our measurements and their 68.3% confidence intervals; dashed lines indicate spectral models with the indicated abundances of the highlighted isotopes relative to the nominal abundance of [Fe/H] = −0.4 dex. The spectra shown in the figure are available as data behind the figure. The package also includes the PHOENIX models used in this work. The data used to create this figure are available.

many astronomical objects because these two isotopologues are typically both optically thin (unlike ^{12}C^{16}O). We find ^{13}CO/C^{18}O = 4.1 ± 1.1 and 6.9 ± 1.8 for GJ 745A and B, respectively.

Although the individual isotopic ratios are nonsolar, our measured ^{13}CO/C^{18}O ratios are broadly consistent with the Solar value of 5.6 ± 0.2 (Lyons et al. 2018) and typical values for the interstellar medium (ISM) in our Galaxy and the disks of other spiral galaxies (ratios of 5–10; Jiménez-Donaire et al. 2017), and are also consistent with values inferred for the ISM in the nuclei of starburst and more quiescent galaxies on 10–100 pc scales (ratios of 2.5–4; Meier & Turner 2004). However, low ^{13}CO/C^{18}O values measured in the ISM of other galaxies are often coincident with low ^{16}O/^{18}O values attributed to abundant ^{18}O (Meier & Turner 2004), the opposite of what we observe for our stars. The isotopic ratios of GJ 745AB are also consistent with young stellar objects (YSOs) and ionized gas regions in our own Milky Way (Smith et al. 2015), but the abundances of these Galactic objects

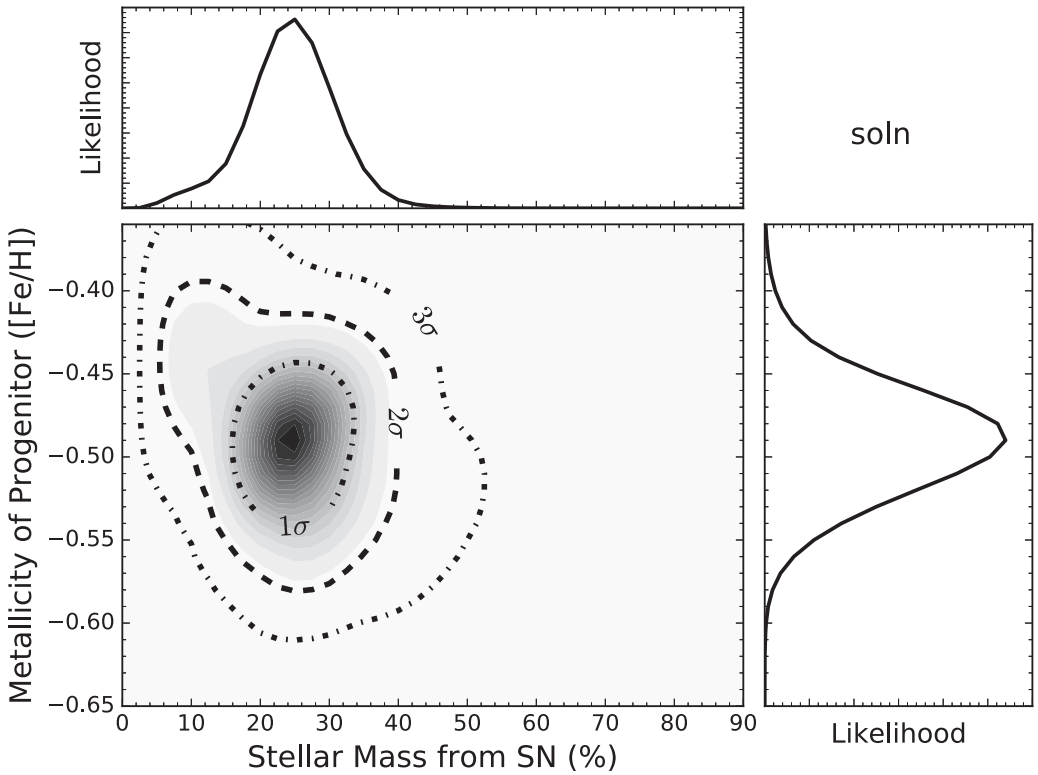

Figure 2. Probability distribution of the initial supernova progenitor's metallicity and the fractional mass contribution of its ejecta to GJ 745AB. Confidence intervals indicated by 1σ, 2σ, and 3σ enclose 68.3%, 95.4%, and 99.73% of the total probability, respectively. The marginalized, 1D distributions of each parameter are also shown. The best-fit values are a 22^{+7}_{-5}% mass contribution and metallicity of $-0.48^{+0.03}_{-0.04}$ dex relative to Solar.

are still inconsistent with GJ 745AB as newly forming stars should have higher metallicity. One must also take care in comparing these to ISM values, as they can be affected by processes such as selective photodissociation (Bally & Langer 1982) and fractionation (Watson et al. 1976), which can lead to the preferential formation or destruction of certain isotopologues of a molecule, such that the measured molecular abundances are not representative of the true abundance of an isotope.

The individual isotopic abundances of our stars cannot be matched by standard models of Galactic chemical evolution (Kobayashi et al. 2011) despite the broad consistency between $^{13}CO/C^{18}O$ in GJ 745A and B and some Galactic measurements. These chemical models predict much higher $^{16}O/^{18}O$ ratios for our observed $^{12}C/^{13}C$ ratio—or equivalently, lower $^{12}C/^{13}C$ ratios at the known stellar metallicity. Some deviations are seen from predictions of the evolution of $^{12}C/^{13}C$ with time and from the observed trends in isotope ratios with Galactic radius. The current $^{12}C/^{13}C$ in the Solar neighborhood ISM is 30% smaller than that in the Sun, with little corresponding change in $^{16}O/^{18}O$ (Milam et al. 2005; Polehampton et al. 2005). There is also a factor of ∼2 dispersion in the present-day $^{12}C/^{13}C$ ratio in the Milky Way ISM at a given Galactic radius (Milam et al. 2005), but this intrinsic scatter is still too small to explain the carbon isotope ratios that we see.

What, then, could cause such surprisingly high isotopic ratios? Different astrophysical phenomena affect $^{12}C/^{13}C$, $^{16}O/^{18}O$, and [Fe/H] in different ways. Accretion of gas enriched by mass-loss products from evolved, asymptotic giant branch stars has been suggested to explain the Sun's oxygen isotope ratios (Gaidos et al. 2009), but this fails to match our observations as these evolved stars have much lower $^{12}C/^{13}C$ ratios than we see (Sneden & Pilachowski 1986). Carbon-rich giant stars of the R Corona Borealis type often have $^{12}C/^{13}C \geqslant 100$ (Fujita & Tsuji 1977) and undergo frequent mass loss (Clayton 1996), but their $^{16}O/^{18}O$ ratios are lower than the Solar value (Clayton et al. 2005), contrary to what we observe. The relatively large $^{12}C/^{13}C$ ratios seen in ultraluminous infrared galaxies (ULIRGs) have been suggested to be due to infall of low-metallicity gas (Casoli et al. 1992a), as is seen in the center of our Galaxy (Riquelme et al. 2010). However, such pristine gas would have too little ^{18}O to reproduce the observed $^{16}O/^{18}O$ ratios in these stars. While a combination of both a starburst (decreasing the $^{16}O/^{18}O$) and an infusion of low-metallicity gas (increasing the $^{16}O/^{18}O$) has been suggested to simultaneously allow for somewhat similar isotopologue ratios ($^{12}CO/^{13}C\,O > 90$, $^{16}O/^{18}O > 900$; König et al. 2016), such a scenario is quite complex.

Alternatively, higher isotopic ratios can be caused by the inclusion of material from dramatic episodes of rapid nucleosynthesis (Casoli et al. 1992b), such as accretion of supernova (SN) ejecta. It is this model that best explains our data. We use models of the evolution of Galactic abundances to represent the initial ISM (Kobayashi et al. 2011) and model the ejecta composition using simulated isotopic yields of a core-collapse supernova (CCSN; Woosley & Weaver 1995). We construct a model in which the free parameters are the initial [Fe/H] of the ISM and SN progenitor star, the progenitor mass, and the fraction of resulting stellar mass consisting of SN ejecta.

We find that enrichment by material from a CCSN with progenitor mass of roughly 21 $M_\odot$ is required to explain our observations, which is independent of the assumed Galactic environment model (Kobayashi et al. 2011)—halo, thick disk,

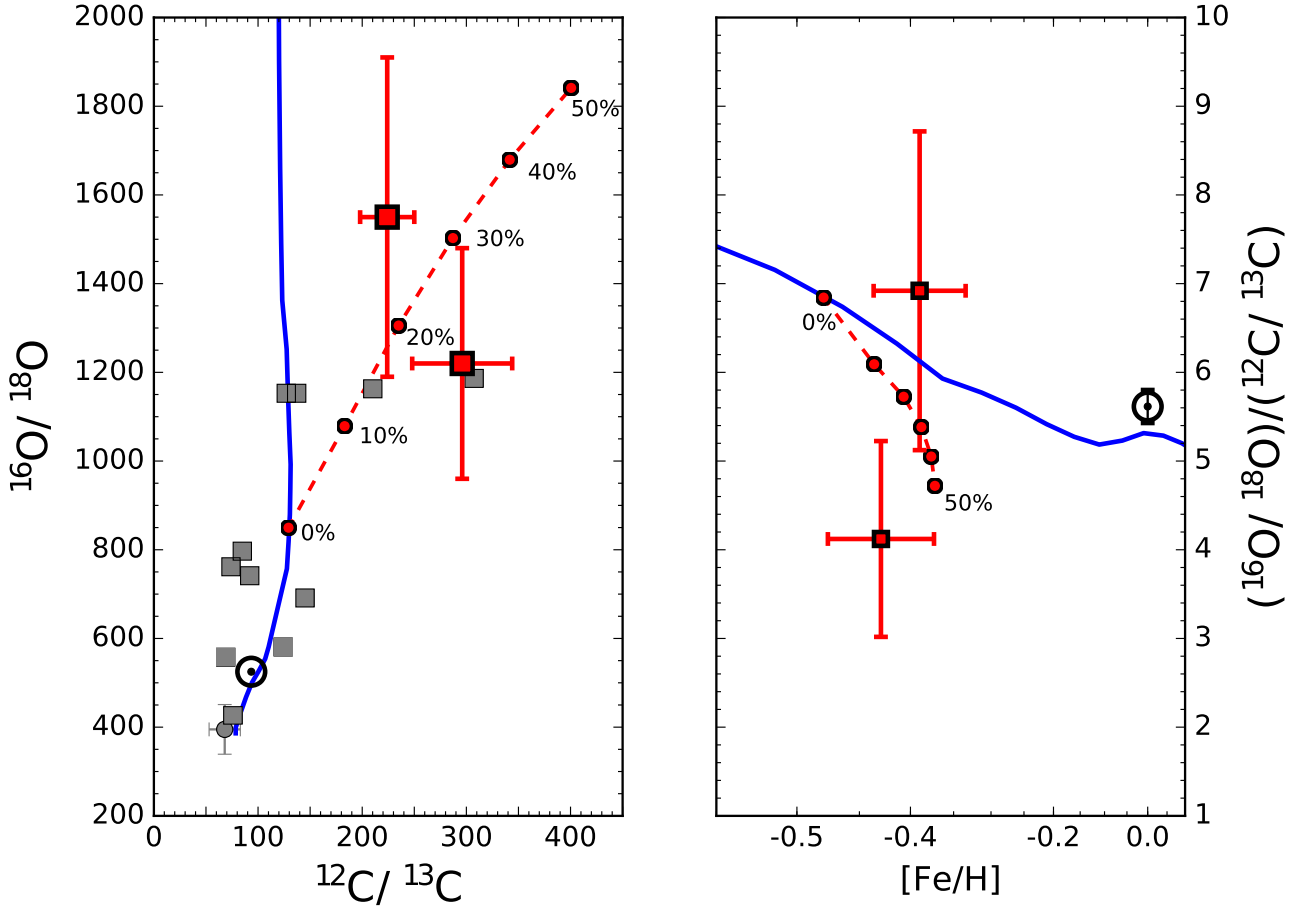

Figure 3. Abundance ratios of M dwarfs GJ745 A and B (red squares) in the context of the Sun (dotted circle; Lyons et al. 2018), local ISM (gray circle; Milam et al. 2005; Polehampton et al. 2005), and YSOs (gray squares; Smith et al. 2015). The M dwarf abundances are inconsistent with models of Galactic chemical evolution (blue line; Kobayashi et al. 2011), but can be explained by substantial mass enrichment from a CCSN (Woosley & Weaver 1995). The red dashed line shows an enrichment track for this progenitor star at intervals of 10% stellar mass contribution to the M dwarf binary. The best fit is 22% enrichment by mass from the ejecta of a 21 $M_{\odot}$ progenitor with initial metal enhancement of −0.48 dex.

Solar neighborhood, or bulge. We can exclude both the thick-disk model and the halo model because GJ 745's 3D motion in the Galaxy ($U = -45.8$ km s^{-1}, $V = +17.3$ km s^{-1}, $W = +22.2$ km s^{-1}) is inconsistent with the motion expected for thick-disk or halo stars (Fuhrmann 2004). We also exclude the bulge model because GJ 745AB is <10 pc away, far from the Milky Way's bulge.

The remaining Solar neighborhood chemical evolution model can explain GJ 745AB's $^{12}C/^{13}C$, $^{16}O/^{18}O$, and [Fe/H] only through enrichment from CCSN ejecta. Our best-fit model requires the injection into a slightly more metal-poor ISM ($[Fe/H] = -0.48^{+0.03}_{-0.04}$) of ejecta from a CCSN progenitor with mass of $21 \pm 1\ M_{\odot}$ and an initial metallicity matching that of the natal ISM, and with 22^{+7}_{-5}% of the M dwarfs' mass consisting of supernova ejecta (see Figures 2 and 3). This mass ratio is lower than predictions that as much as half of the Sun's carbon could have come from supernova ejecta (Clayton 2003), albeit with a different progenitor mass and composition. Though such mass fractions may seem large, half the mass of GJ 745AB (0.3 $M_{\odot}$) would represent just 0.4% of the total ejected mass from such a supernova. If the enrichment came from multiple supernovae over a short period of time, their individual contributions would be even less.

This example of strongly enriched star formation is not unprecedented, as the isotopic ratios of GJ 745A and B (though not their [Fe/H]) are also consistent with those measured for a handful of YSOs such as IRS 43 (Smith et al. 2015). If these objects and the GJ 745AB binary formed in large part from SN ejecta, high-resolution abundance analyses (Souto et al. 2018) should clearly reveal that formation path, e.g., via enhanced abundances of elements produced by rapid nucleosynthesis (the "*r*-process;" Cowan et al. 1991). Deeper observations should also enable detection of $^{12}C^{17}O$, which our observations did not have the sensitivity to detect. The direct comparison of three O isotopic abundances in a single star would enable a determination of the level of mass-dependent isotopic fractionation as has been done for many objects in the solar system (Clayton & Nittler 2004).

Observing the CO fundamental rovibrational band at high resolution has several clear advantages over similar, past observations of dwarf stars (Pavlenko & Jones 2002; Tsuji 2016): (1) we observe the rarer species in the CO fundamental band, where the cross-sections of these rare isotopologues are greatest; (2) we resolve individual lines so blending is not a limitation; and, as a result, (3) we are sensitive to much lower abundances of ^{13}CO and $C^{18}O$. The fundamental band lines of the CO isotopologues are visible from spectral types G to L (Allard 2014); modern facilities could easily measure isotopic abundances in substellar brown dwarfs, and the next generation of giant ground-based telescopes could extend this work to the realm of extrasolar planets. The obvious downsides to our

approach are the amount of observing time required per star and the small number of operational high-resolution, *M*-band-capable spectrographs. Nonetheless, such instruments may be poised to open a new window on stellar isotopic patterns and on our Galaxy's chemical enrichment history.

The authors wish to thank many colleagues, as well as the anonymous referee, for stimulating and thought-provoking discussions that improved the quality of this Letter: T. Barman, Z. Maas, J. Birkby, G. Smith, H. Knutson, C. Pilachowski, I. Roederer, B. Svoboda, J. Teske, M. Veyette, and E. Newton. Author contributions: conceptualization: I.C.; data curation: I.C.; formal analysis: I.C., B.F., J.V., R.F.; funding acquisition: I.C.; investigation: I.C., B.F., J.L., J.V., X.G., B.M.; methodology: I.C., J.L.; project administration: I.C.; resources: I.C., J.L.; software: I.C., B.F., J.L., J.V.; supervision: I.C.; validation: I.C., J.L.; visualization: I.C.; writing—original draft: I.C., B.F., J.L., E.M.; writing—review and editing: all authors. Competing interests: Authors declare no competing interests. Data and materials availability: raw IRTF data will be available for download from the observatory data archive, https://irsa.ipac.caltech.edu/applications/irtf/. The final, calibrated spectra of GJ745 A and B and the PHOENIX models used in this Letter are available in FITS format. The authors wish to recognize and acknowledge the very significant cultural role and reverence that the summit of Mauna Kea has always had within the indigenous Hawaiian community. We are most fortunate to have the opportunity to conduct observations from this mountain.

Facility: IRTF (iSHELL).

ORCID iDs

J. D. Lothringer https://orcid.org/0000-0003-3667-8633
E. A. C. Mills https://orcid.org/0000-0001-8782-1992
J. Valverde https://orcid.org/0000-0002-2345-8888
A. Skemer https://orcid.org/0000-0001-6098-3924

References

Allard, F. 2014, in IAU Symp. 299, Exploring the Formation and Evolution of Planetary Systems, ed. M. Booth, B. C. Matthews, & J. R. Graham (Cambridge: Cambridge Univ. Press), 271
Avni, Y. 1976, ApJ, 210, 642
Bailer-Jones, C. A. L., Rybizki, J., Fouesneau, M., Mantelet, G., & Andrae, R. 2018, AJ, 156, 58
Bally, J., & Langer, W. D. 1982, ApJ, 255, 143
Benedict, G. F., Henry, T. J., Franz, O. G., et al. 2016, AJ, 152, 141
Casoli, F., Dupraz, C., & Combes, F. 1992a, A&A, 264, 49
Casoli, F., Dupraz, C., & Combes, F. 1992b, A&A, 264, 55
Clayton, D. 2003, Handbook of Isotopes in the Cosmos (Cambridge: Cambridge Univ. Press), 326
Clayton, D. D., & Nittler, L. R. 2004, ARA&A, 42, 39
Clayton, G. C. 1996, PASP, 108, 225
Clayton, G. C., Herwig, F., Geballe, T. R., et al. 2005, ApJL, 623, L141
Cowan, J. J., Thielemann, F.-K., & Truran, J. W. 1991, PhR, 208, 267
Cushing, M. C., Vacca, W. D., & Rayner, J. T. 2004, PASP, 116, 362
Cutri, R. M., Wright, E. L., Conrow, T., et al. 2012, Explanatory Supplement to the WISE All-Sky Data Release Products, Technical Report, http://wise2.ipac.caltech.edu/docs/release/allsky/expsup/index.html
Dressing, C. D., & Charbonneau, D. 2015, ApJ, 807, 45
Fuhrmann, K. 2004, AN, 325, 3
Fujita, Y., & Tsuji, T. 1977, PASJ, 29, 711
Gaia Collaboration, Brown, A. G. A., Vallenari, A., et al. 2018, A&A, 616, A1
Gaidos, E., Krot, A. N., & Huss, G. R. 2009, ApJL, 705, L163
Gaidos, E., & Mann, A. W. 2014, ApJ, 791, 54
Goorvitch, D. 1994, ApJS, 95, 535
Hase, F., Wallace, L., McLeod, S. D., Harrison, J. J., & Bernath, P. F. 2010, JQSRT, 111, 521
Houdebine, E. R. 2010, MNRAS, 407, 1657
Husser, T.-O., Wende-von Berg, S., Dreizler, S., et al. 2013, A&A, 553, A6
Jao, W.-C., Henry, T. J., Gies, D. R., & Hambly, N. C. 2018, ApJL, 861, L11
Jenkins, J. S., Ramsey, L. W., Jones, H. R. A., et al. 2009, ApJ, 704, 975
Jiménez-Donaire, M. J., Cormier, D., Bigiel, F., et al. 2017, ApJL, 836, L29
Kobayashi, C., Karakas, A. I., & Umeda, H. 2011, MNRAS, 414, 3231
König, S., Aalto, S., Muller, S., et al. 2016, A&A, 594, A70
Lyons, J., Gharib-Nezhad, E., & Ayres, T. 2018, NatCo, 9, 908
MacDonald, J., & Gizis, J. 2018, MNRAS, 480, 1711
Mann, A. W., Feiden, G. A., Gaidos, E., Boyajian, T., & von Braun, K. 2015, ApJ, 804, 64
Meier, D. S., & Turner, J. L. 2004, AJ, 127, 2069
Milam, S. N., Savage, C., Brewster, M. A., Ziurys, L. M., & Wyckoff, S. 2005, ApJ, 634, 1126
Newton, E. R., Charbonneau, D., Irwin, J., & Mann, A. W. 2015, ApJ, 800, 85
Pavlenko, Y. V., & Jones, H. R. A. 2002, A&A, 396, 967
Polehampton, E. T., Baluteau, J.-P., & Swinyard, B. M. 2005, A&A, 437, 957
Rayner, J., Tokunaga, A., Jaffe, D., et al. 2016, Proc. SPIE, 9908, 990884
Riquelme, D., Bronfman, L., Mauersberger, R., May, J., & Wilson, T. L. 2010, A&A, 523, A45
Rothman, L., Gordon, I., Barber, R., et al. 2010, JQSRT, 111, 2139
Skrutskie, M. F., Cutri, R. M., Stiening, R., et al. 2006, AJ, 131, 1163
Smith, R. L., Pontoppidan, K. M., Young, E. D., & Morris, M. R. 2015, ApJ, 813, 120
Sneden, C., & Pilachowski, C. A. 1986, ApJ, 301, 860
Souto, D., Cunha, K., García-Hernández, D. A., et al. 2017, ApJ, 835, 239
Souto, D., Unterborn, C. T., Smith, V. V., et al. 2018, ApJL, 860, L15
Tsuji, T. 2016, PASJ, 68, 84
Vacca, W. D., Cushing, M. C., & Rayner, J. T. 2004, PASP, 116, 352
Watson, W. D., Anicich, V. G., & Huntress, W. T., Jr. 1976, ApJL, 205, L165
Woosley, S. E., & Weaver, T. A. 1995, ApJS, 101, 181